Prediction of Laser-Spot-Weld Shape by Numerical Analysis and Neural Network

W.-S. CHANG and S.-J. NA

The finite element method (FEM) and neural network were applied for predicting the bead shape in laser spot welding of type 304 thin stainless steel sheets. The parameters of pulsed Nd:YAG laser spot welding such as pulse energy, pulse duration, sheet metal thickness, and gap between sheets were varied for various experiments and numerical simulations. The penetration depth and nugget size of spot welds measured for specimens without gap were compared with the calculated results to verify the proposed finite element model. Sheet metal thickness, gap size, and bead shape of the workpiece without gap were selected as the input variables for the back-propagation learning algorithm of the neural network, while the bead shape of the workpiece with and without gap was considered as its output variable. Various combinations of stainless steel sheet metal thickness were considered to calculate the laser-spot-weld bead shape of the workpiece without gap, which was then used as the input variable of neural network to predict the bead shape for various gap sizes. This combined model of finite element analysis and neural network could be effectively applied for the prediction of bead shapes of laser spot welds, because the numerical analysis of laser spot welding for the workpiece with gap between two sheets is highly limited.

I. INTRODUCTION

LASER beam welding is a field of growing importance in industry. It is particularly useful in cases where localized heating is desired. There are many outstanding advantages in using laser welding as the bonding method of choice over other bonding technologies. Compared to common adhesive bonding or soldering used in joining processes, laser welding offers a number of attractive features such as high weld strength–to–weld size ratio, reliability, and minimal heat-affected zone. These provide the benefits of low heat distortion, noncontact process, repeatability, ability to automate, and high throughput.

A wide range of research activities has been undertaken, including laser beam delivery systems and mechanical behavior of laser-welded sheet steels. However, research on the dimension of laser beam welds for a given metal thickness has not been extensively studied. The weld pool dimension and weld quality of spot welds produced by using a pulsed Nd:YAG laser welding machine depend on various process parameters such as spatial intensity distribution of the incident laser beam, peak power of pulse, pulse energy, pulse time, and temporal shape of beam power during the pulse. When developing the welding procedure for a specific application, each of these parameters must be characterized and fully specified. This is usually done by using empirical techniques, since most analytical and numerical models for laser weld pool development ignore various aspects of the laser-material interaction,[1] thus making it difficult to accurately predict the weld pool shape.

W.-S. CHANG, Senior Member of Research Staff, is with the Precision Machining Group, Korea Institute of Machinery & Materials, Taejon 305-343, Korea. S.-J. NA, Professor, is with the Department of Mechanical Engineering, Korea Advanced Institute of Science and Technology, Taejon 305-701, Korea.

Manuscript submitted September 29, 1999.

Previous Model of Laser Welding

Many models were proposed on laser welding to produce reliable predictions of temperature distributions that are of great importance for in-depth analysis and eventual improvement of the process.

The quasi-stationary temperature field in the workpiece was calculated analytically by introducing a moving line source of heat. In 1977, Cline and Anthony[2] integrated the point source over the workpiece surface to yield a Gaussian power distribution, eliminated singularities in the temperature calculations, and showed that the spot size has a strong influence on the maximum temperature occurring in the workpiece. The model assumed 100 pct absorption and calculated an exponential decrease of temperature in the vertical direction. Both the conduction and keyhole welding condition were considered, whereas weld pool convection was not included in the model. A simpler approach is to compensate for the weld pool convective heat transfer with an artificially high thermal conductivity of material in the weld pool. Typically, a thermal conductivity of 10 times as much as its actual value at the solidus temperature has been used in conventional welding models.[3]

The difficulties associated with analytical models of the laser welding process may be partially overcome by employing numerical rather than purely analytical techniques. Since detailed information on temperature-dependent thermophysical properties is difficult to obtain, however, most of the numerical modeling efforts have assumed constant values for selected thermophysical properties.

Mazumder and Steen[4] developed the first numerical model of the continuous laser welding process. This model implemented the finite difference technique for a Gaussian beam intensity distribution and started with the assumption that the absorptivity of the incident radiation below the boiling point was 20 pct. While the convective flow in the

weld pool and the temperature dependence of thermophysical properties were not considered, the nonlinearities of convection and radiation to surroundings were included in the model. The absorptivity of laser radiation was considered to be 100 pct when the temperature exceeded the boiling point. As a result, matrix points remained in the conducting network at fictitiously high temperatures to simulate the convection and radiation heat transfer mechanisms within the plasma.

Recently, there are studies of transient behavior of the temperature distribution in a solid heated by short powerful laser pulses[5] and thermal analysis correlated with experiments.[6] It was based on a three-dimensional model of the laser heating problem in which the temperature-dependent coupling between the laser pulse and sample and the temperature-dependent thermal characteristics of the sample were fully taken into account. Limited experimental studies of the effect of Nd:YAG laser process parameters on laser spot weld dimensions and weld quality have been reported.[7,8]

This study was performed to predict the bead shape in laser spot welding of AISI type 304 stainless steel sheets. AISI type 304 stainless steel has many advantages such as low thermal conductivity, high resistance to corrosion, and high stability at elevated temperature. Due to these advantages, AISI type 304 stainless steel is used in numerous industries, including electronics, medical instruments, home appliances, automotive, and specialized tube industry. Moreover AISI type 304 stainless steel is a superior absorber of laser light. Consequently, slightly higher weld penetration depths can be achieved than with carbon steels for a given welding condition. Another advantage of using a laser to weld stainless steels is the low weld distortion produced by the low general heat input and the laser weld shape. Typical applications include electron guns for television tubes, razor blades, optoelectronic transmitters, and food mixer whisks.[9]

The finite element method (FEM) and neural network were applied for predicting the bead shape in laser spot welding of AISI type 304 stainless steel sheets with thickness less than 1 mm. The penetration depth, nugget size, and bead width of laser spot welds were measured for specimens with and without gap and compared with the predicted results to verify the proposed model.

II. FINITE ELEMENT ANALYSIS

A. *Physical Description of Model*

When using a pulsed-mode laser, the welding process becomes somewhat more complicated than just a simple diffusion of heat away from the surface. When a high-power beam initially strikes the surface, a significant amount of material may be vaporized forming a small hole known as a keyhole. Laser energy that subsequently enters the hole is trapped and carried deeper into the material than would otherwise be the case. Pulsed Nd:YAG lasers can also be used efficiently in this process by employing a pulse consisting of a very high-power initial spike of short duration, approximately 100 μs, followed by much lower irradiance for the remainder of the pulse. The peak power during the spike is sufficient to create the initial keyhole, but during the rest of the pulse, the power is insufficient to cause further vaporization. However, the material round the keyhole melts and

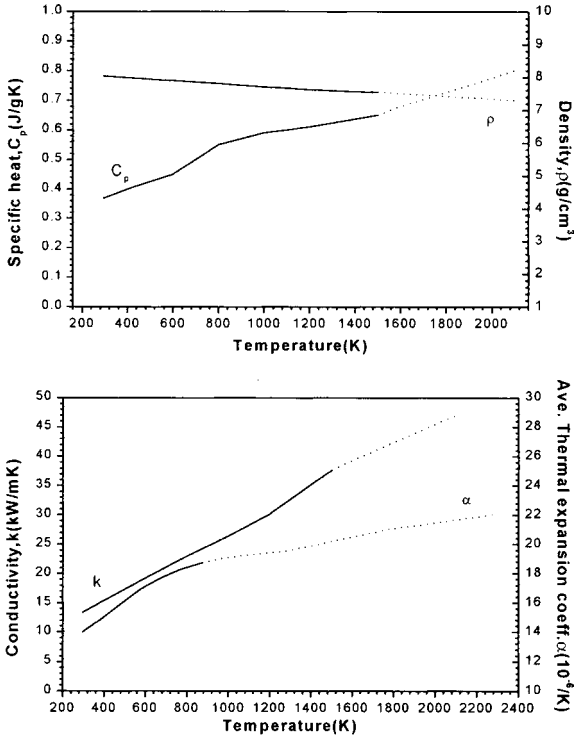

Fig. 1—Temperature-dependent thermal properties.

fills in the hole. Since the absorption of energy within the keyhole is not greatly dependent on the condition and type of metal surface, this type of action enables materials with high melting points to be welded.[10,11]

The following assumptions were made in the formulation of the finite element model.

(1) The workpiece is initially at 20 °C. Both the laser beam and coordinate mesh are fixed.
(2) At temperatures below the boiling point of the material (*i.e.*, 2500 °C for stainless steel), a proportion of the incident radiation is absorbed, depending on the absorptivity and the rest is reflected. Above the boiling point, radiation absorbed by the vapor/plasma is ignored.
(3) When the temperature of nodes exceeds the boiling point of stainless steel, it remains in the mesh at the vaporization temperature to simulate the presence of a plasma-filled keyhole, and the thermophysical properties for iron vapor at 2500 °C[5] are used.
(4) All thermophysical properties for AISI type 304 stainless steel are considered to be temperature dependent, as shown in Figure 1.
(5) The latent heat of fusion and vaporization for AISI type 304 stainless steel is considered according to Matsuhiro *et al.*[12]

B. *Governing Equation and Boundary Conditions*

The heat transfer of laser spot welding can be calculated by applying heat conduction theory, and the thermal and mechanical aspects of the problem can be decoupled without imposing a significant penalty on the calculation accuracy. The assumptions on this are that dimensional changes during laser spot welding are not significant and that the mechanical

work done is negligible compared to the thermal energy changes. The energy equation of the problem is

$$\rho(T)C(T)\frac{\partial T}{\partial t} = \nabla \cdot (K(T)\nabla T) + Q(x,y,z) \qquad [1]$$

The natural boundary condition can be defined by

$$k_n \frac{\partial T}{\partial n} - q + h(T - T_0) + \sigma\varepsilon(T^4 - T_0^4) = 0 \qquad [2]$$

where the film coefficient used was $h = 10$ W/m^2 K and the emissivity value of 0.25 was assumed for stainless steel.[14] The heat flux specified on the workpiece surface is given by incident laser beam. During laser spot welding in atmosphere, heat losses from the workpiece surface are through natural convection, radiation, and evaporation of molten metal. Only the convective and radiative heat losses were applied for this study. The initial condition for the transient analysis is $T(x,y,z,0) = T_0(x,y,z)$, where T_0 is the initial temperature.

C. *Volumetric Heat Absorption*

In the simplest case, the beam power absorbed locally at the keyhole wall can be described by considering only the Fresnel absorption of the beam intensity distribution $I(x,y,z)$ hitting the surface. The intensity of the laser beam has a Gaussian-like distribution:[13,15]

$$I(x,y,z) = I(r,z) = I_0(t)\left(\frac{r_f}{r_{f0}}\right)^2 \exp\left(-\frac{2r^2}{r_f^2}\right) \qquad [3]$$

where I_0 is the beam intensity at the beam's focal point (W/m^2), r_{f0} the beam's focal radius (m), r_f the beam's radius at depth z (m), and r the radial distance from center of the beam (m). The peak intensity I_0 is expressed as follows:

$$I_0 = \frac{2P(t)}{\pi {r_{f0}}^2} \qquad [4]$$

where $P(t)$ is the time-dependent laser power at the center point. The pulsed laser beam has a very-high-power initial spike with short duration of 100 μs followed by much lower irradiance for the remainder of the pulse. The value of $P(t)$ can be expressed by

$$\begin{aligned} P(t) &= P_h t/t_s, && 0 \le t \le t_s \\ &= P_h(2t_s - t)/t_s, && t_s \le t \le 3t_s/2 \\ &= P_l && 3t_s/2 \le t \le t_p \end{aligned} \qquad [5]$$

The final form of the volumetric heat source term, $Q(x,y,z,t)$, can be expressed as

$$Q(x,y,z,t) = Q(r,z,t) = \frac{2P(t)(1-R)}{\pi {r_{f0}}^2 d}\left(\frac{r_f}{r_{f0}}\right)^2 \exp\left[-\frac{2r^2}{r_f^2}\right] \cdot u(z) \qquad [6]$$

where $u(z)$ is the Kronecker delta function; that is,

$$\begin{aligned} u(z) &= 1, \text{ from surface to vaporization depth } (d) \\ &= 0, \text{ otherwise} \end{aligned}$$

At the centerline of the workpiece, the temperature gradient in the transverse direction can be neglected due to the symmetry of heat flow. The amount of volumetric heat is determined by vaporization depth.

D. *Vaporization Depth*

If the laser-beam irradiance is so high that the temperature of the material reaches its boiling point, a significant amount of surface material will be removed. The rate of removal can be estimated by employing a simple energy balance arrangement. A semi-infinite solid is considered for a rate of heat flow H into the unit area of the surface. It is supposed that vaporization will cause the material surface to move inward at a velocity v_s. Thus, a mass of material equal to $v_s\rho$ will be removed in unit time. The total amount of energy required to convert a mass m at the initial temperature T into a vapor can be written as follows:

$$E_v = m(C_s(T_m - T) + C_L(T_v - T_m) + L_f + L_m) \qquad [7]$$

In this equation, the usual relationships of parameters are $L_f \ll L_v$, $T \ll T_v$, and $C_s \approx C_L = C$. To calculate the mass of vaporized material, its volume is assumed to form a conelike shape, whose volume is given by $V = (1/3)\pi r^2 d$, where r is the effective beam radius and d the vaporization depth.

Thus, the heat flow required to support a surface velocity of v_s is given by

$$H = \frac{1}{3}v_s\rho(CT_v + L_v) \qquad [8]$$

where $H = E_v/t_p\pi r^2$ is the beam intensity and $v_s = d/t$ the vaporization velocity.

Consequently, the vaporization depth is calculated by

$$d = \frac{3Ht}{\rho(CT_v + L_v)} \qquad [9]$$

E. *Material Properties*

As previously noted, the material to be joined is AISI type 304 stainless steel sheet. Temperature-dependent thermal properties of this material were assumed to be isotropic and homogeneous and are shown in Figure 1. Since thermal properties over the melting point are not known, linearly extrapolated properties were used in the simulation. The latent heat of fusion was 247 kJ/Kg, to be released or absorbed over the temperature range from $T_S = 1400$ °C to $T_L = 1500$ °C, and the latent heat of vaporization was 7600 kJ/kg.[12]

F. *Description of Discrete Model*

To simulate the pulsed laser spot welding process, a three-dimensional thermal analysis was used. To consider the temperature-dependent parameters in the formulation of the laser spot welding process, the model relied on solving a nonlinear parabolic differential equation for heat diffusion. The nonlinear finite element solver, ABAQUS, was employed to solve the transient thermal analysis of the problem. The peak temperature reached the boiling point so that the phase change needed to be considered. The specimen was taken

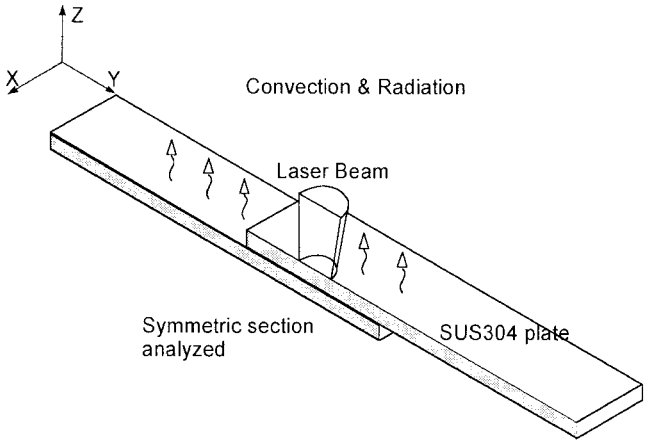

Fig. 2—Symmetric physical model for thermal analysis of laser spot welding.

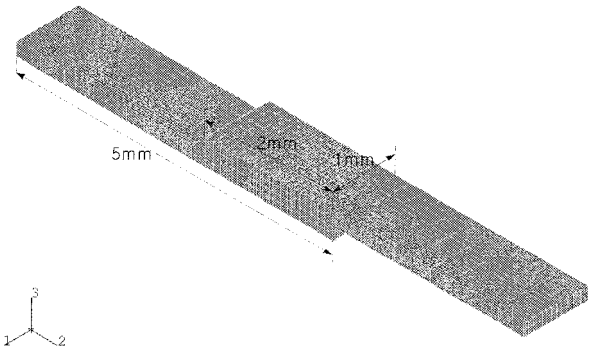

Fig. 3—Finite element thermal model of laser spot welding.

in the form of two flat plates connected at the joint part. The overall geometry and boundary conditions of the solution domain are shown schematically in Figure 2.

Since the symmetry of this problem is evident, just a half part of the plates was modeled, based on eight-node quadratic three-dimensional solid elements in the finite element analysis. The mesh size was approximately 90 μm near the centerline of the laser beam at which the large temperature gradient was steep. The mesh generation used in the simulations is shown in Figure 3.

The time-step was controlled according to the criterion that the temperature change between any two adjacent time-steps was less than 500 K. The analysis was done up to 4 seconds, when the temperature inside the specimen was expected to cool down approximately to 373 K.

III. NEURAL NETWORK

A. *Back-Propagation Algorithm*

The architecture of the neural network for the selection of laser welding parameters consisted of three parts. The first part was the specification of the welding condition and the second one the hidden layer regarded as a black box. The last part was an output layer for setting up the laser welding parameters. The schematic diagram of the neural network for predicting the lap welded joint shape, composed of the penetration depth, nugget size, and bead width, is

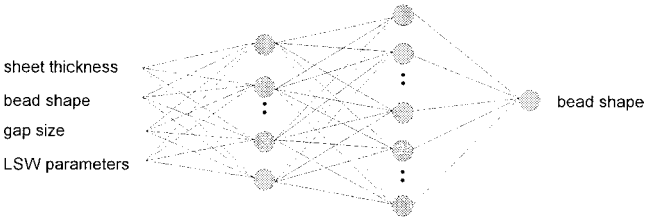

Fig. 4—Schematic diagram of neural network for estimating bead shape.

shown in Figure 4. The range of experimental data used to train the proposed neural network structure is shown in Table I, and the number of training data was 20 in each thickness of base metal

The performance of the neural network depends on the number of hidden layers and the number of nodes in the hidden layer.[16] The structure of the neural network applied for estimating the welding conditions was chosen by the trial and error method.

B. *Selection of Appropriate Input Variables to the Neural Network*

Three different combinations of process parameters were considered to determine the appropriate input variables to the neural network. Laser spot welding process parameters (focal length, energy, and pulse time), sheet metal thickness (upper and lower plate), and gap size and bead shape (penetration depth and nugget size) of the workpiece without gap were selected as the input variables for the back-propagation learning algorithm of the neural network, while the bead shape (penetration depth and nugget size) of the workpiece with various gap sizes was considered as its output variable. In type 1, all of the variables mentioned were selected as the input variables, while, in type 2, the sheet metal thickness (upper and lower plate), gap size, penetration depth, and nugget size and, in type 3, only the gap size, penetration depth, and nugget size were selected as the input variables.

IV. EXPERIMENTS

Experiments were designed to determine the input and output variables appropriate to the neural network. The experimental requirements are shown in Table II and the experimental setup for Nd:YAG laser spot welding is shown in Figure 5. Specimens with gap were set by various gap gages. A pulse-type Nd:YAG laser welding machine was used for all experiments. The beam oscillator was capable of the maximum output power of 400 W. Type 304 stainless steel specimens with five different combinations of thickness (0.3 + 0.33 mm, 0.33 + 0.5 mm, 0.4 + 0.6 mm, 0.6 + 0.5 mm, and 0.5 + 0.5 mm) were prepared for the experiments. Exposure of stainless steel sheet to a laser pulse formed a spot weld, which was then sectioned and prepared to measure the fusion zone dimensions. Some typical morphologies of the sectioned specimen are shown in Figure 6.

V. RESULTS AND DISCUSSIONS

Transient temperature contours in the workpiece simulated at various processing times are shown in Figure 7. For clarity, the contours are presented only in the joint region

Table I. Range of Experimental Data Used to Train Neural Network

Combination of Specimen Thickness (mm)	Range of Weld Parameters					
	Nugget Size (mm)	Penetration Depth (mm)	Focal Length (mm)	Gap Size (mm)	Energy (J)	Pulse Duration (ms)
0.3 + 0.33	0.33 to 0.56	0.34 to 0.78	+2, +1	0	2.5 to 3.5	2, 4, 6
0.33 + 0.5	0.32 to 0.61	0.45 to 0.87	+2, +1	0.06	2.5 to 3.5	2, 4, 6
0.4 + 0.6	0.37 to 0.61	0.55 to 0.93	+2	0.12	3.0 to 5.0	2, 6
0.5 + 0.5	0.37 to 0.55	0.7 to 1.0	+2		3.0 to 5.0	2, 6
0.5 + 0.6	0.35 to 0.46	0.84 to 1.0	+2		3.0 to 5.0	2, 6

Table II. Experimental Requirements for Laser Spot Welding of Specimen

Specimen Thickness (mm)		Focal Length (mm)	Gap Size (mm)	Energy (J)	Pulse Duration (ms)
Upper	Lower				
			0	2.5	2.0
0.3	0.33	+2		3.0	
0.33	0.5		0.06	3.5	4.0
0.4	0.6	+1		4.0	
0.5	0.5		0.12	5.0	6.0
0.6	0.5				

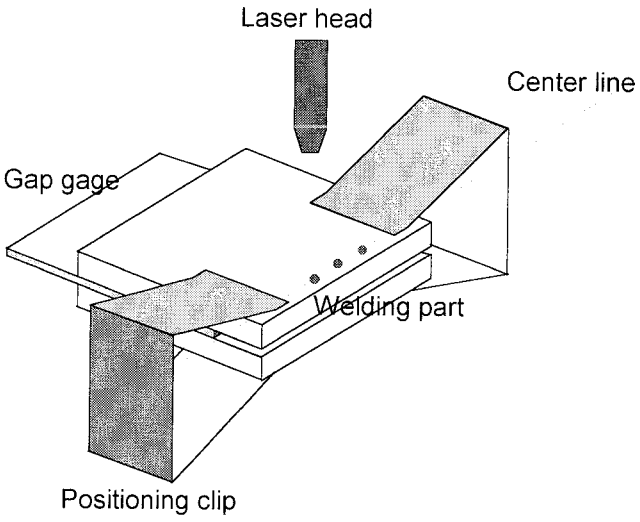

Fig. 5—Experimental setup of laser spot welding.

herein. The contours were obtained for the pulse duration of 4 ms at the beam energy of 2.5 J, and they cover those of the initial heating, melting, and cooling stages. A relatively high temperature occurs near the upper plate of the joint, which is considered to be the result of a high power spike beam heating the top surface. The peak temperature calculated in the weld metal is considerably higher than the melting temperature, which is probably caused by neglecting the convective motion in the weld pool. During the cooling stage after 4 s, the temperature distribution becomes relatively even.

Experimental and simulated results were compared first on single-pulse spot welds with changing laser spot size. The model was run for both the duration of the laser pulse and the subsequent cooling period. Figure 8 shows a typical comparison example of cross sections of experiments and simulations obtained for the thickness combination of 0.3 + 0.33 mm with laser energy of 2.5 J and pulse time of 4 ms. It is shown that the nugget size and penetration depth calculated (Figure 8(a)) agree well with the experimental result (Figure 8(b)) with the error of about 4 pct, while the top bead width calculated is about 17 pct narrower than the experimental one. It is probably due to the fact that the temporal pulse shape, plasma formation, and laser-material interaction influence the formation of the top bead that the latter cannot be considered in the developed finite element model. However, the top bead size is less important in determining weld quality, such as joining strength, than the nugget size and penetration depth.

Figure 9 shows the calculated result and the micrograph of the cross section of the spot weld obtained with different focal positions. In this case, the focal point was located 1 mm above the plate, while it was 0.5 mm for the results of Figure 8. It is also shown that the nugget size and penetration depth calculated (Figure 9(a)) agree with the experimental result (Figure 9(b)) within an error of about 6 pct. This micrograph shows that the penetration depth is smaller than the former one, which also appears in the numerical results. This comparison has shown that the penetration depth associated with pulsed laser welding is changing drastically as the focal position varies. Previous works have shown that the deepest penetration is achieved when the focal point is located 2 to 3 mm below the surface of the workpiece.[17]

Various combinations of stainless steel sheet metal thicknesses were considered to calculate the laser spot weld bead shape of the workpiece without gap, which would then be used as the input variable of the neural network for predicting the bead shape of sheet metals with various thicknesses and gap sizes. To test the calculated results, experimental and calculated joint shapes were compared for various welding conditions (Figures 10 and 11). It is shown that the FEM simulations can predict the penetration depth and nugget size within a maximum error of about 7 pct when there is no gap between sheets.

With these experimental results, the prediction of the bead shape using the neural network was performed to determine the appropriate input variable combination. Figure 12 shows that the error of predicted nugget size and penetration depth determined by comparing them with experimental ones is less than 15 pct for type 1 of the neural network, where the focal length, pulse energy, pulse time, sheet metal thickness (upper and lower plate), gap size, penetration depth, and nugget size were selected as the input variables.

Figures 13 and 14 show that the neural network model of types 2 and 3 can estimate the bead shape of laser spot welds such as nugget size and penetration depth almost as

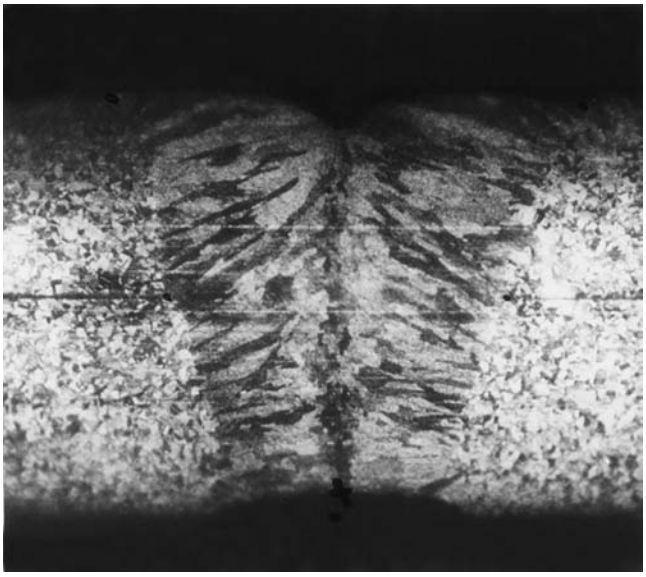

(*a*) No gap

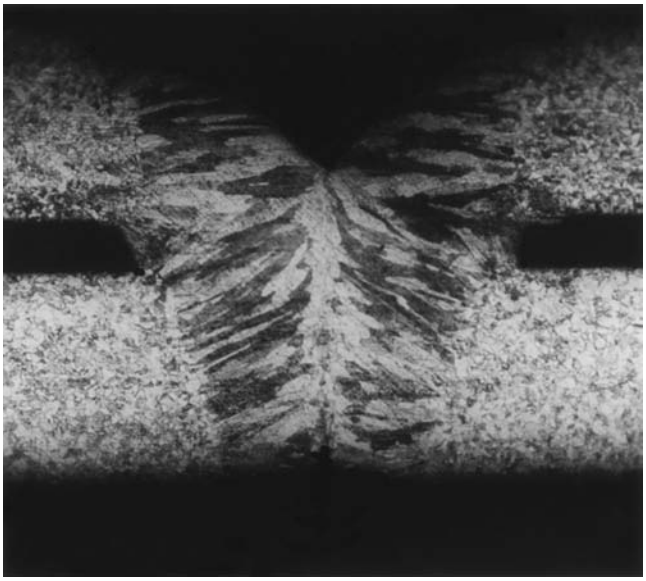

(*b*) Gap = 60 μm

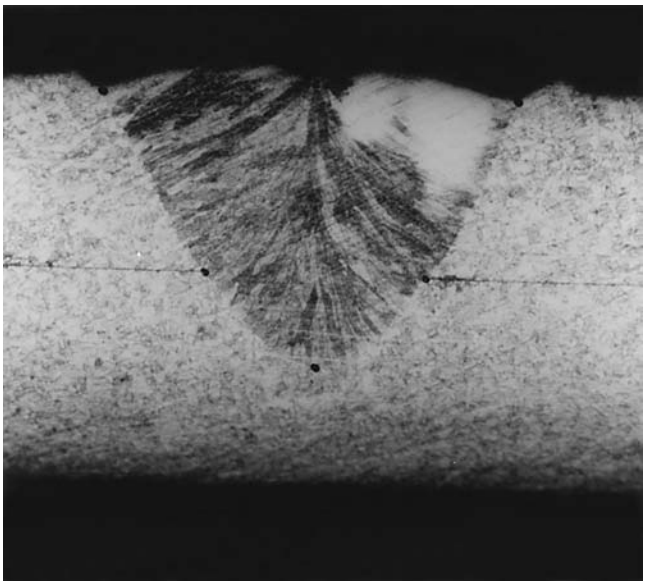

(*c*) No gap

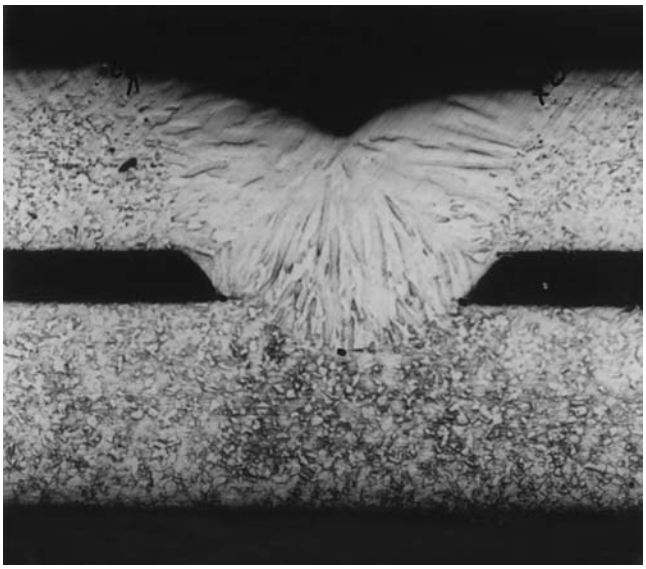

(*d*) Gap = 60 μm

Fig. 6—Morphologies of sectioned specimen with various conditions. (*a*) and (*b*) Energy = 3.5 J, pulse duration = 6 ms, spot size = 500 μm. (*c*) and (*d*) Energy = 2.5 J, pulse duration = 4 ms, and spot size = 600 μm.

well as that of type 1. These results show that the process parameters adopted in types 2 and 3 are also appropriate as input variables to the neural network.

Figure 15 shows the error of nugget size and penetration depth predicted by using the combined model of finite element analysis and neural network. The predicted results were compared with the experimental ones of the specimen of 0.5 + 0.5 mm thickness combination with various gap sizes. It shows that the error was less than 10 pct. From these results, it was shown that the combined model of FEM analysis and neural network could be effectively applied for the prediction of spot weld bead shape such as nugget size and penetration depth for the workpiece pairs with various gap sizes.

VI. CONCLUSIONS

From the results of the finite element analysis, neural network, and experiments for laser spot welding of thin stainless steel sheets, the following conclusions may be drawn.

1. The proposed finite element model can estimate the laser spot weld bead shape of thin stainless steel sheets within a maximum error of about 7 pct, if they are layered tightly without gap between them.
2. The developed neural network, which uses the bead shape data calculated for the specimen without gap and a few geometrical data of specimen with gap, can predict the

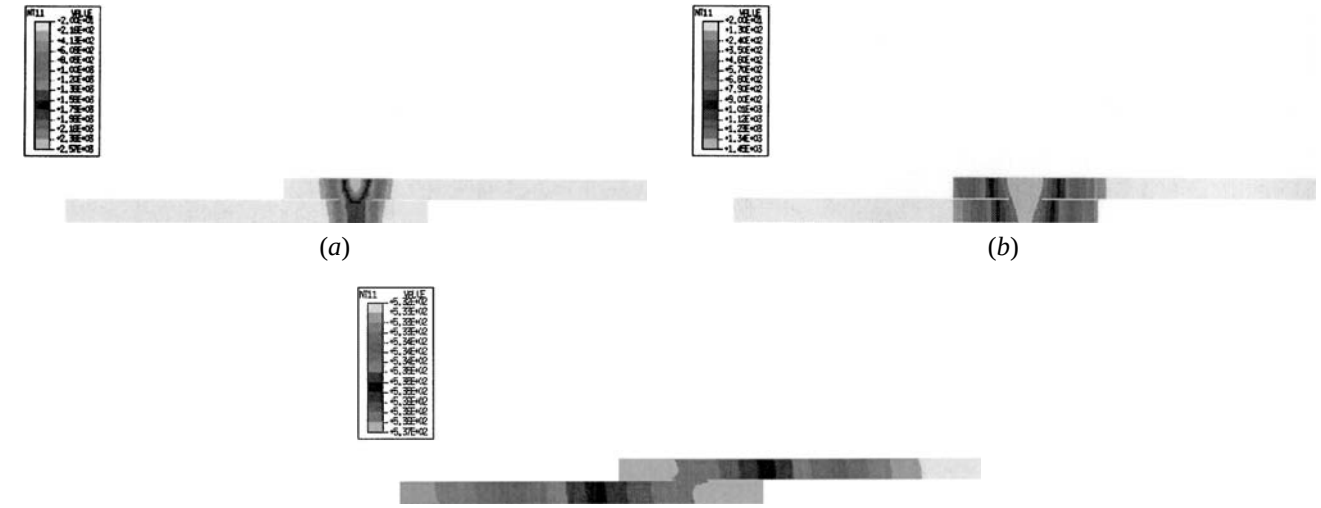

(*a*) (*b*) (*c*)

Fig. 7—Temperature contours calculated at various times for energy of 2.5 J and pulse duration of 4 ms: (*a*) 4 ms—end of pulse duration, (*b*) 20 ms, and (*c*) 4 s.

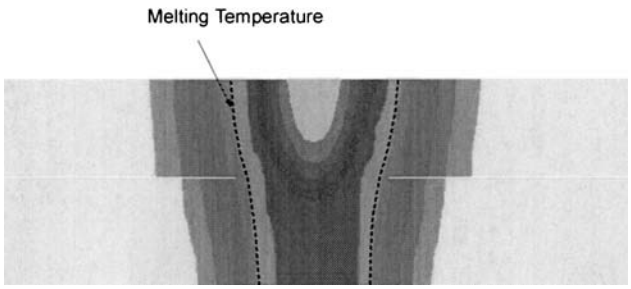

(*a*)

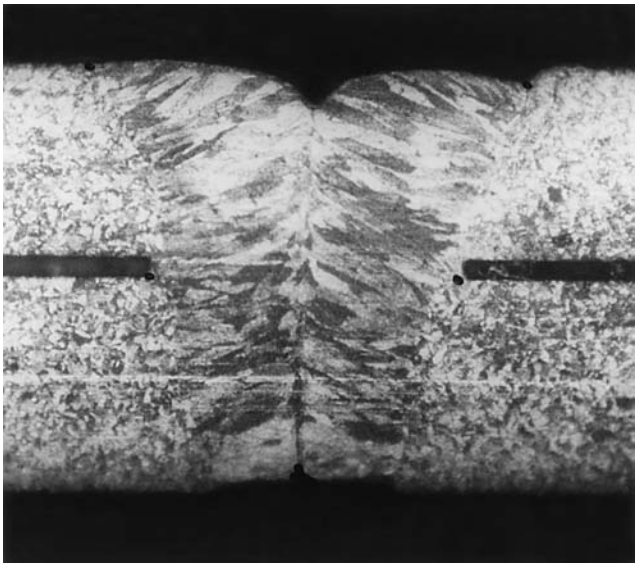

(*b*)

Fig. 8—Comparison of calculated result with experimental one for energy of 2.5 J, pulse duration of 4 ms, focal position of +0.5 mm, and specimen thickness of 0.3 + 0.33 mm. (*a*) Contour of calculated melting temperature and (*b*) sectioned specimen.

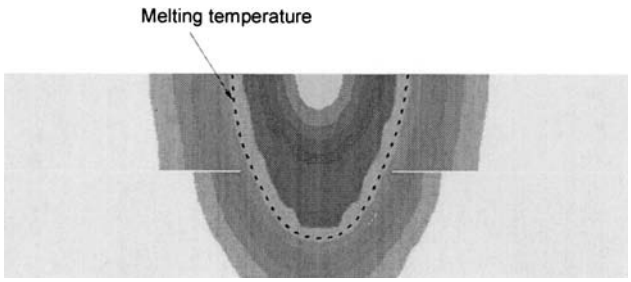

(*a*)

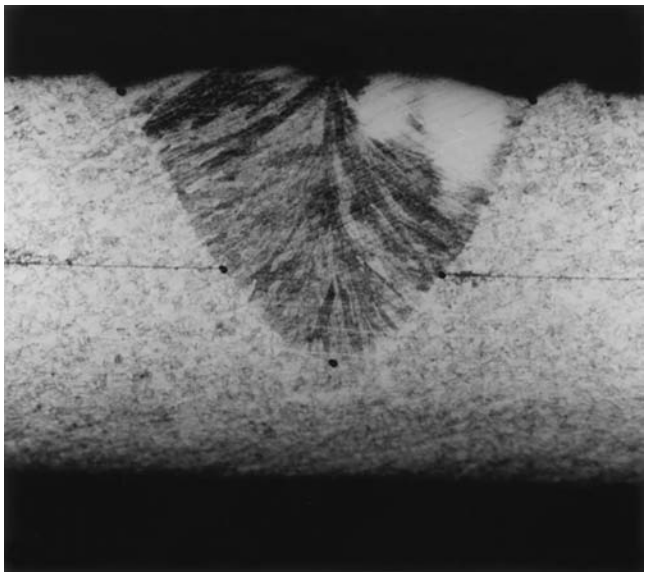

(*b*)

Fig. 9—Comparison of calculated result with experimental one for energy of 2.5 J, pulse duration of 4 ms, focal position of +1.0 mm, and specimen thickness of 0.3 + 0.33 mm. (*a*) Contour of calculated melting temperature and (*b*) sectioned specimen.

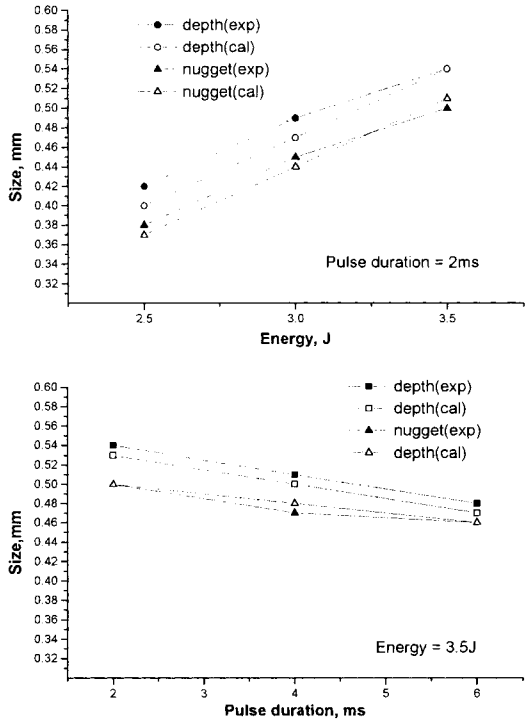

Fig. 10—Comparison of numerical results with experimental ones for sheet thickness combination of 0.3 + 0.33 mm.

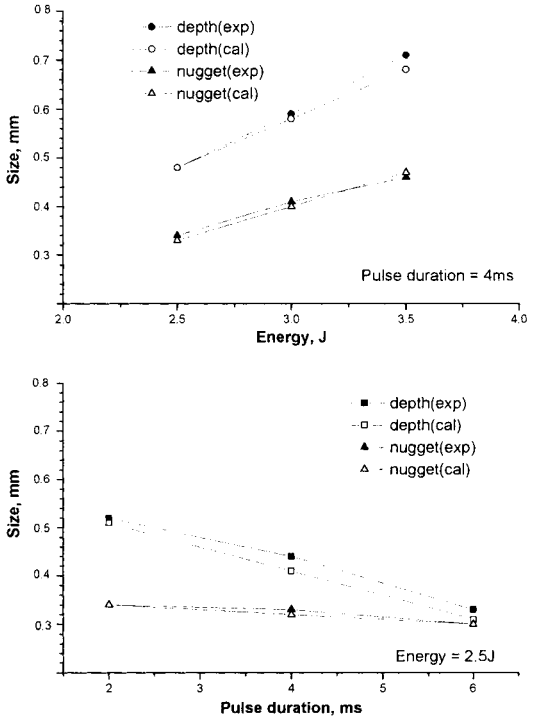

Fig. 11—Comparison of numerical results with experimental ones for sheet thickness combination of 0.33 + 0.5 mm.

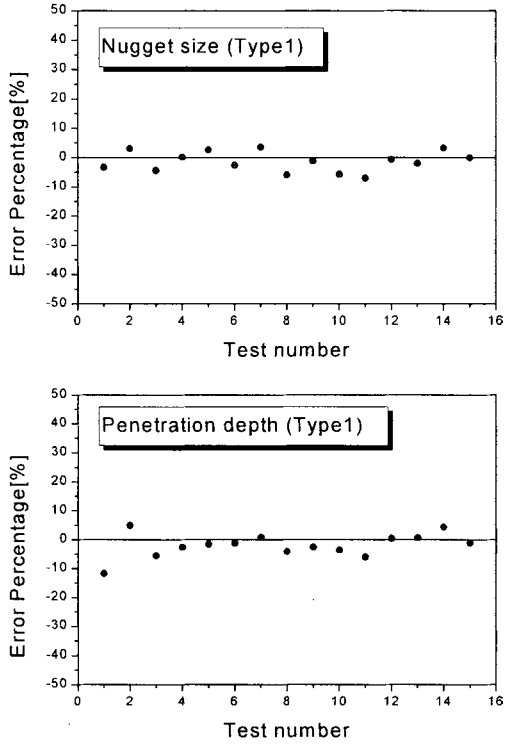

Fig. 12—Error of bead shape predicted by type 1 neural network.

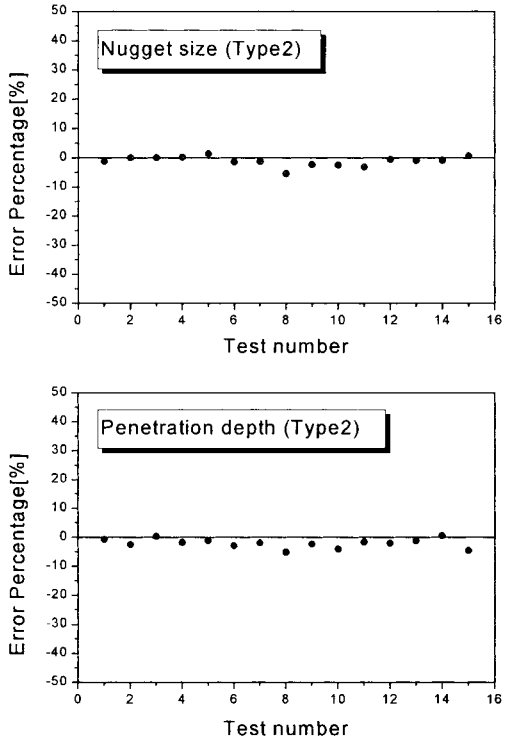

Fig. 13—Error of bead shape predicted by type 2 neural network.

laser spot weld bead shape of thin stainless steel sheets with various gap sizes within an error less than 10 pct.

3. The combined model of finite element analysis and neural network can be effectively applied for the prediction of laser spot weld bead shapes, because the numerical analysis of laser spot weld bead shape for the workpiece with gap between two sheet metals is highly limited.

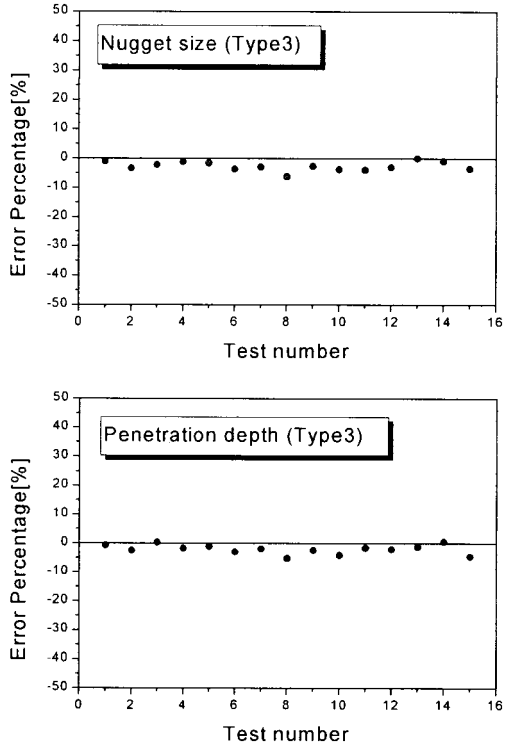

Fig. 14—Error of bead shape predicted by type 3 neural network.

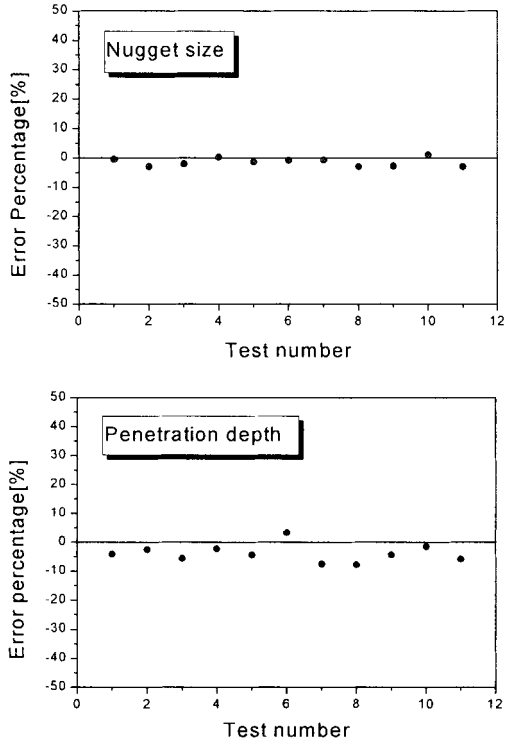

Fig. 15—Error of bead shape predicted by combined model of FEM and neural network.

NOMENCLATURE

$C(T)$	temperature-dependent specific heat capacity (J kg^{-1} K^{-1})
$\rho(T)$	temperature-dependent density (kg m^{-3})
$K(t)$	temperature-dependent thermal conductivity (W m^{-1} K^{-1})
Q	power generation per unit volume in the domain (W m^{-3})
F	focusing number
H	beam intensity (W m^{-2})
M	beam quality number
k_n	thermal conductivity normal to surfaces that are subject to radiation, convection, and imposed heat fluxes (W m^{-1} K^{-1})
h	heat transfer coefficient for convection (W m^{-2} K^{-1})
σ	Stefan–Boltzmann constant for radiation (W m^{-2} K^{-4})
ε	emissivity
T_0	ambient temperature (K)
q	heat flux (W m^{-2})
P_h	peak power of initial pulse spike (W)
P_l	lowered average power (W)
t_s	initial pulse spike duration (s)
t_p	total pulse duration (s)
d	vaporization depth (m)
C_s	solid specific heat capacity (J kg^{-1} K^{-1})
C_L	liquid specific heat capacity (J kg^{-1} K^{-1})
T_m	melting point (K)
T_v	boiling point (K)
L_f	latent heat of fusion (kJ kg^{-1})
L_v	latent heat of vaporization (kJ kg^{-1})

REFERENCES

1. J. Mazumder and D. Voekel: *Proc. LAMP '92*, Japan High Temperature Society, Osaka, Japan, 1992, pp. 373-80.
2. H.E. Cline and T.R. Anthony: *J. Appl. Phys.*, 1977, vol. 48, pp. 3895-3900.
3. D.C. Weckman, L.C. Mallory, and H.W. Kerr: *Z. Metallkd.*, 1989, vol. 80, pp. 459-68.
4. J. Mazumder and W.M. Steen: *J. Appl. Phys.*, 1980, vol. 51, pp. 941-47.
5. O.O.D. Neto and C.A.S. Lima: *J. Phys. D: Appl. Phys.*, 1994, vol. 27, pp. 1785-1804.
6. M.R. Frewin and D.A. Scott: *Welding J.*, 1999, vol. 1, pp. 15s-22s.
7. J.T. Liu, D.C. Weckman, and H.W. Kerr: *Metall. Trans. B*, 1993, vol. 24B, pp. 1065-76.
8. H.N. Bransch, D.C. Weckman, and H.W. Kerr: *Welding J.*, 1994, vol. 73, pp. 141s-151s.
9. C. Dawes: *Laser Welding*, Abington Publishing, Cambridge, United Kingdom, 1992, pp. 31-53.
10. J. Wilson and J.F.B. Hawkes: *Lasers: Principles and Applications*, Prentice-Hall International(UK) Ltd., Hertfordshire, United Kingdom, 1987, pp. 166-89.
11. W.M. Steen: *Laser Material Processing*, Springer-Verlag, Berlin, 1991, pp. 108-44.
12. Y. Matsuhiro, Y. Inaba, and T. Ohji: *Jpn. Welding Soc.*, 1993, vol. 11, pp. 479-83.
13. C. Lampa, A. Kaplan, J. Powell, and C. Magnusson: *J. Phys. D: Appl. Phys.*, 1997, vol. 30, pp. 1293-99.
14. P. Tekriwal and J. Mazumder: *Welding J.*, 1988, vol. 67, pp. 150s-156s.
15. A. Kaplan: *J. Phys. D: Appl. Phys.*, 1994, vol. 27, pp. 1805-14.
16. S.C. Chapra and R.P. Canale: *Numerical Method for Engineers*, 2nd ed., McGraw-Hill Book Co., New York, NY, 1988, pp. 358-61.
17. M.R. Frewin and D.A. Scott: *Proc. ICALEO '95*, Laser Institute of America, Orlando, FL, 1995, pp. 904-13.